Impact of Core Architecture on Solution Properties of Dendrimer-like Star Copolymers

Cheryl M. Stancik,[†] John A. Pople,[‡] Mikael Trollsås,[⊥] Peter Lindner,[§] James L. Hedrick,[⊥] and Alice P. Gast*[,†,#]

Department of Chemical Engineering, Stanford University, Stanford, California 94305; Stanford Synchrotron Radiation Laboratory, Stanford Linear Accelerator Center, PO Box 4349, Stanford, California 94309; IBM Almaden Research Center, 650 Harry Road, San Jose, California 95120; and Institut Laue-Langevin, 156 Avenue des Martyrs, F-38042 Grenoble, Cedex 9, France

Received September 9, 2002; Revised Manuscript Received February 7, 2003

ABSTRACT: We present a small-angle neutron scattering study of a series of isomeric dendrimer-like star copolymers investigated in solution. Each copolymer consists of a highly branched core with linear partially deuterated polymer chains emanating from the outermost generation to create a starlike copolymer. By studying the copolymers in solvents contrast matched to the outer starlike chains, we focus our study on the effects of the core branching architecture. In our dilute solution data analysis we use models to obtain analytical expressions for the form factor of the copolymer cores. We find the core radius of gyration and fractal dimension depend on the core branching architecture. From our semidilute data we obtain experimental structure factors and see evidence of liquidlike structuring in some copolymers. Thus, the architectural features of these isomeric copolymers have an impact on both the conformation of and interactions between these molecules in solution.

I. Introduction

The rich variety of polymer architectures created by both nature and synthetic polymer chemists has enabled a field of study that explores the complex relationships between the physical properties of molecules and their macromolecular topology. Although the effects of branching in polymers have long been recognized as an important area of study,[1,2] the ability to control branching architecture has only recently been achieved. Over the past two decades, dramatic advances in polymer synthesis have provided a means to control polymer architecture on the molecular length scale, thus allowing the creation of a variety of novel macromolecules and the opportunity to experimentally investigate the effects of polymer architecture.

Dendrimers, which are polymer molecules with regularly placed branching junctures cascading in "generations" from a central core, were first synthesized in the 1980s[3−5] and have been gaining the attention of polymer scientists due to their unique properties.[6−8] Both theoretical and experimental studies have shown that the details of these complex architectures, including the number of generations and the nature of the spacer group between branching junctures, affect the conformation and characteristic dimensions of dendrimer molecules in solution.[8]

In another highly branched architecture, star polymers are characterized by polymer chains emanating from a central core, but in this case all the branching occurs near the center of the core. Daoud and Cotton[9] and Birshtein and Zhulina[10,11] investigated the unique architecture of star polymers using scaling approaches revealing that a range of concentration regimes exists within individual molecules, producing more than one characteristic length scale. The inhomogeneous density distribution created as a consequence of this architecture leads to an increase of the osmotic pressure inside a star polymer as the concentration of polymers in solution is increased.[12] This leads to an osmotic repulsion, which in turn induces ordering phenomena in star polymer solutions near the overlap concentration. Ordering in star polymer solutions has been experimentally observed using neutron scattering studies.[13−18] Furthermore, star polymer solutions have been the subject of theoretical studies which have allowed an enriched understanding of the phenomena observed in scattering studies.[13,19] These studies show that effective pair potentials can be used to describe the interactions that lead to liquidlike ordering, allowing star polymers to be viewed as "ultrasoft" colloidal particles.[13] Thus, star polymers exhibit a dual nature as they have characteristics of both polymers and colloidal particles.[14,17,20,21]

These polymers of well-defined branched architecture have given promise to a host of applications once thought unachievable due to the stochastic nature of traditional syntheses. Polymer architectures employing dendrimer structures are attractive candidates for drug delivery as they have well-defined size and a high degree of functionality, allowing them to mimic multifunctional biological molecules.[22] In the development of therapeutics for the treatment for prion disease, dendritic molecules were able to stimulate normal cellular mechanisms to destroy the infectious proteins while their linear analogues gave no such response.[23] Various hyperbranched architectures employing polyester dendritic scaffolds are under investigation as carriers for anticancer drugs based on promising initial results.[24,25] These studies emphasize the important relationship between polymer architecture and the ability to deliver polymeric drugs to a desired site.

† Stanford University.
‡ Stanford Linear Accelerator Center.
⊥ IBM Almaden Research Center.
§ Institut Laue-Langevin.
# Present address: Department of Chemical Engineering, Massachusetts Institute of Technology, Cambridge, MA 02139.
* Corresponding author: e-mail gast@mit.edu.

10.1021/ma021450+ CCC: $25.00
Published on Web 06/26/2003

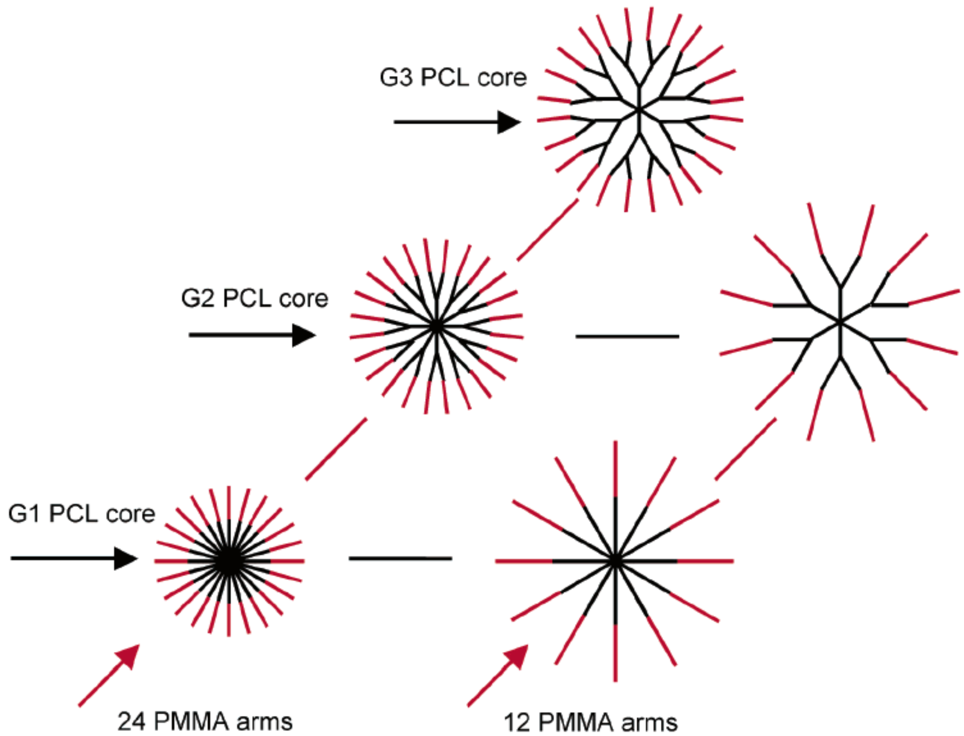

Figure 1. Isomeric PCL−PMMA dendrimer-like star copolymer series is schematically shown. The black lines show the branching architecture of the PCL core while the red lines show the d_5-PMMA arms.

The geometry of hyperbranched polymers has proven useful in the development of advanced materials. One unique feature of dendrimer and star architectures is their ability to encapsulate a functional moiety within the core of their structures, giving potential for site isolation.[6,26−29] Fréchet et al. have explored how architecture impacts the ability to achieve site isolation in both dendritic and star polymers with porphyrin cores.[26,29] Using this approach, a chromophore-labeled dendrimer was prepared for single-layer light-emitting diode applications.[28] In an application for microelectronics, IBM has developed methods to use hyperbranched molecules as pore generators en route to the formation of nanoporous ultralow dielectric materials after they determined that linear molecules of the same composition gave poor properties.[30−32]

To exploit the unique features of hyperbranched molecules, we must gain a deeper understanding of how their architecture relates to their properties. Only recent control of polymer branching has permitted studies of well-defined branched polymers.[29,33−40] In our research program, we work to elucidate the relationships between macromolecular architecture and the underlying polymer physics controlling the solution and bulk properties of materials. Specifically, we focus our efforts on understanding the effects of macromolecular architecture on the solution properties of highly branched, novel hybrid architectures combining linear polymers with starlike dendrimer cores using small-angle neutron scattering (SANS).

In the study presented in this paper, we investigate how architectural features, such as branch juncture placement and branch length within the core of a star molecule, affect the behavior of dendrimer-like star block copolymers in solution. We have the opportunity to study isomeric molecules having the same degree of polymerization and composition, thus differing only in architecture. First we study the dilute solution properties of the copolymers and consider how core and arm architecture impact the overall dimensions of the core. We then characterize their interactions as the concentration is increased in an effort to assess the influence of the architecture of a branched core on the structure and properties of the star copolymer emanating from it.

II. Experimental Section

II.1. Copolymer Materials. Using synthetic procedures that allow control of macromolecular architecture, both the placement of branching junctures and the degree of polymerization of the polymer chains that connect these branching junctures can be designed. This series of dendrimer-like block star copolymers was prepared using a combination of ring-opening polymerization (ROP) of poly(ϵ-caprolactone) ($(CH_2)_5$-OCO, PCL) and atom transfer radical polymerization (ATRP) of poly(methyl methacrylate) (PMMA) as described previously.[41] ROP provides the means to make highly uniform star and dendrimer-like star structures having oligomeric or polymeric chains between each branching junction with well-defined end group functionality that can be readily transferred into an initiator for ATRP. The PMMA is partially deuterated ($CD_2C(CD_3)(COOCH_3)$, d_5-PMMA) to allow for contrast matching in neutron scattering experiments. These copolymers each have nearly the same overall molecular weight and composition with PCL polymer chains emanating from a central core and d_5-PMMA chains attached to the outermost PCL chains. As schematically shown in Figure 1, branching junctures are placed in different locations within the PCL core to create generation 1 (G1) (i.e., star architecture), generation 2 (G2), or generation 3 (G3) architecture cores as presented before.[39] The d_5-PMMA chains are attached by one end to the outermost chains of these cores to create a star copolymer.

Multifunctional initiators create the templates for the core of the molecules and the first generation of the "living" ROP of the PCL monomers. In this series of polymers, 6, 12, or 24 PCL chains were grown from these central core initiators. To create the G2 and G3 core architectures, branching junctures were introduced by derivatizing the chain ends with an AB_2 moiety followed by ROP of PCL in successive steps to achieve

Table 1. Characteristics of PCL−PMMA Dendrimer-like Star Copolymers

	PCL core architecture				PMMA arm architecture			copolymer properties	
copolymer	generation	DP[a] branch[b]	M_n[c] (g/mol)	M_w/M_n[d]	f[e]	DP[a] arm[b]	M_w/M_n[d]	M_n[c] (g/mol)	M_w/M_n[d]
G1-12	G1	50	69 700	1.04	12	69	1.26	156 000	1.13
G2-12	G2	33	69 800	1.15	12	69	1.08	150 000	1.42
G1-24	G1	25	71 100	1.08	24	34	1.32	180 000	1.20
G2-24	G2	17	71 400	1.12	24	34	1.10	145 000	1.27
G3-24	G3	14	71 500	1.19	24	34	1.19	145 000	1.45

[a] Degree of polymerization. [b] Target values. [c] As determined by ^{1}H NMR end group analysis. [d] As determined by size exclusion chromatography. [e] Functionality or number of arms.

the desired number of generations. The degree of polymerization of the PCL chains was controlled so that each core contained a total of ~600 PCL units. This synthetic technique results in structures with target molecular weights and narrow polydispersities (1.04−1.19). Further details regarding the synthesis and characterization of these cores can be found in the literature.[39,42−45] Confirmation of the desired architectures and molecular weights was achieved using NMR investigations. In these NMR studies, end group analysis of the synthetic intermediates and final products verified that the target structures were achieved.

This PCL core design allows us to focus on the effects of the architectural variations in branch placement and length in the core of the copolymer star. The PCL chains of the outermost generation were capped with functional groups that act as initiators for the ATRP of the PMMA chains. In this series either 12 or 24 PMMA chains were grown from the PCL core with target degree of polymerizations of 69 or 34 to yield a total of ~820 PMMA repeat units in each molecule, respectively. The synthetic conditions were optimized to prevent the coupling of PCL cores during the ATRP of the starlike PMMA chains. To consider the success of the ATRP synthesis, the PCL cores of these copolymers were degraded according to literature procedures,[41] allowing direct study of the PMMA arms. Our studies show PMMA polydispersities typical of an ATRP synthesis (1.08−1.32), indicating good initiator efficiency. The molecular weights for the final copolymer products were assessed using NMR. The characteristics of this copolymer series are summarized in Table 1. Further details of the synthetic procedures and characterization can be found elsewhere.[41]

II.2. Sample Preparation. Copolymer solutions for the SANS experiments were prepared at concentrations ranging from 0.2 to 15 wt % in toluene. Hydrogenated toluene (Sigma-Aldrich, 99.5+% A.C.S. Reagent) and deuterated toluene (D_8, Cambridge Isotopes Laboratories, D 99.6%) were used as received. The scattering length density (ρ) of a molecule with z atoms is calculated from the following expression:

$$\rho = \frac{\delta N_A}{M}\sum_{i=1}^{z} b_z \qquad (1)$$

Here, δ is the partial specific density of the molecule in the chosen solvent, N_A is Avogadro's constant, M is the molecular weight, and b_z is the coherent neutron scattering length of the nucleus z. For neutron scattering, the contrast between the components of a system is defined as the square of the difference of the scattering length densities of these components. For example, the contrast for a system comprising components A and B is given as $(\Delta\rho)^2 = (\rho_A - \rho_B)^2$. A solvent mixture of hydrogenated and deuterated toluene was prepared such that the scattering length density of the solvent matched that of the partially deuterated d_5-PMMA polymer, leaving the observed neutron scattering signal from the PCL cores alone.[46] The d_5-PMMA contrast matched toluene mixture was prepared by mass and thoroughly mixed. This toluene mixture was then used to prepare the copolymer samples by mass. Shortly after preparation, samples were transferred to the sample cells for the SANS experiments.

II.3. SANS: Data Collection and Reduction. Scattering experiments were performed on the 30 m instrument (NG3) at the National Institute of Standards and Technology (NIST) Center for Cold Neutron Research (Gaithersburg, MD) and on the 80 m instrument (D11) at Institut Laue-Langevin (ILL) (Grenoble, France). For each experiment, the sample-to-detector distance was chosen in order to obtain the desired range of the momentum transfer, q, defined as $q = (4\pi/\lambda)\sin(\theta/2)$, where θ is the scattering angle. For all SANS experiments the temperature was maintained at 25 °C.

SANS experiments on copolymers G1-12, G1-24, G2-12, and G2-24 were performed at NIST at a wavelength of $\lambda = 0.6$ nm with a wavelength spread of $\Delta\lambda/\lambda = 0.150$. The detector was offset 20 cm to give a larger q range. A sample to detector distance of 530 cm was used for copolymers G1-12, G2-12, and G2-24, giving a q range of 0.07−1.00 nm^{-1}. For copolymer G1-24 the sample-to-detector distance of 310 cm gave a q range of 0.13−2.00 nm^{-1}. Samples contained in 1 mm cells with quartz windows provided by NIST had transmissions of about 0.80. The two-dimensional intensity data were corrected and radially averaged to obtain one-dimensional scattering data on an absolute scale using correction and reduction routines developed at NIST.[47]

SANS experiments on copolymer G3-24 were performed at ILL with a wavelength of $\lambda = 0.6$ nm with a wavelength spread of $\Delta\lambda/\lambda = 0.09$. Two sample-to-detector distances of 250 and 1000 cm were used, giving a q range of 0.06−1.50 nm^{-1}. Samples were contained in 1 mm quartz cells (Hellma, 404-QS) with Teflon caps to prevent loss of solvent with transmission values comparable to those at NIST (0.85−0.88). Again, the two-dimensional intensity data were corrected, and radial averaging was performed to obtain one-dimensional scattering data on an absolute scale using data correction and reduction routines developed at ILL.[48]

II.4. Small-Angle Neutron Scattering: Data Analysis. The contribution to the scattering due to the sample cell is removed from the one-dimensional data obtained using the reduction procedures provided by the scattering facilities. Solvent scattering is subtracted on a volume fraction basis. For a solution of identical particles, the coherent scattering intensity, $I(q)$, can be expressed as follows:

$$I(q) = \phi V_W P(q)\, S(q) = \frac{N_A}{(\Delta\rho)^2}\frac{d\Sigma^{coh}}{d\Omega}(q) \qquad (2)$$

In this expression, ϕ is the polymer volume fraction, V_W is the weight-average polymer molar volume, $P(q)$ and $S(q)$ are the form and structure factors, respectively, $(\Delta\rho)^2$ is the neutron contrast, and $d\Sigma^{coh}/d\Omega\ (q)$ is the coherent macroscopic differential scattering cross section. The form factor, $P(q)$, contains contributions to the scattering intensity due to interference effects within an individual scattering center and therefore gives information about the size and shape of the scattering centers. Analytical expressions have been developed for many common shapes and will be discussed further in section III.2. The structure factor, $S(q)$, arises from interference effects between different scattering centers and provides information about the interaction potential and local organization of scattering centers. To decompose the total scattering intensity into the form factor and structure factor, we make use of the decoupling approximation[34] and assume that the particles are centrosymmetric and that the intra- and interparticle effects can be separated.[49] These approximations have

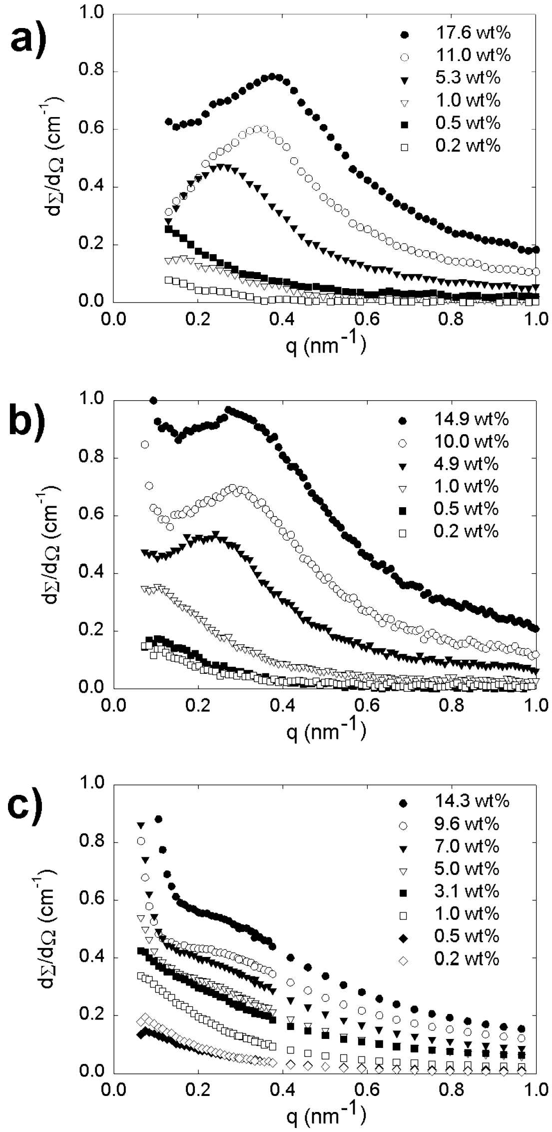

Figure 2. SANS profiles are shown for dendrimer-like star copolymers: (a) G1-24, (b) G2-24, and (c) G3-24.

been successfully applied for other hyperbranched and star systems.[18,34]

III. Results and Discussion

III.1. Qualitative Scattering Data. In Figure 2 we display the scattering data for three copolymers, G1-24, G2-24, and G3-24, each studied at concentrations ranging from dilute to semidilute. All three copolymers have 24 [d_5-PMMA]$_{34}$ arms emanating from the chain ends of the outermost generation of the PCL cores and therefore differ only in their core architecture. The scattering profile arises from the PCL core, as the solvent was matched to the d_5-PMMA chains; however, although the d_5-PMMA do not contribute to the scattering intensity, their presence affects the shape of the scattering profile as they interact with one another and the PCL cores. It is immediately evident the differences in core architecture have a pronounced effect on the features of the scattering profile. In all cases, the increase in polymer concentration leads to either an inflection or a peak in the scattering profile, indicating that more structure is developing in the solution as the polymers begin to interact.

In the case of copolymer G1-24, all the polymer chains emanate from the central core like a star molecule.

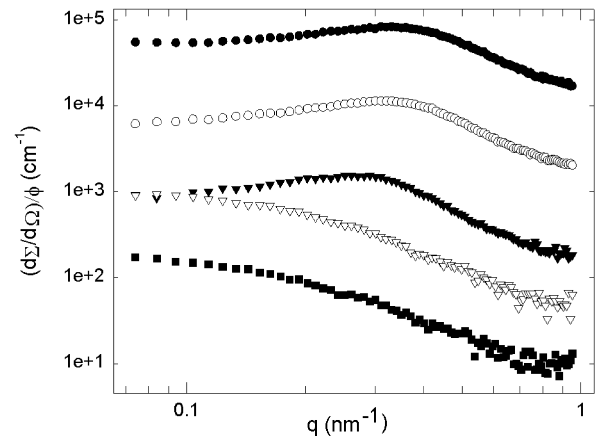

Figure 3. SANS profiles for copolymer G1-12 normalized by polymer volume fraction are shown. The copolymer concentrations of the data sets are 15.0 wt % (closed circles), 9.1 wt % (open circles), 5.0 wt % (closed triangles), 0.5 wt % (open triangles), and 0.2 wt % (closed squares) from top to bottom, respectively. Each data set is offset by a multiple of 10.

Scaling theory predicts that this architecture results in a very inhomogeneous distribution of the polymer segments within the molecule with a high density at the core of the molecule due to the connectivity of the chains to the central branching point.[9] Consequently, the polymer chains in a star architecture are subjected to two competing forces: the osmotic pressure within the polymer and the elastic free energy of chain stretching. In other words, chains stretch in order to relieve the internal osmotic pressure created by the high concentration of segments connected to the core, yet there is a free energy penalty for this chain stretching as this results in deviation from the random coil state. As investigated theoretically by Witten and co-workers,[50] the steep rise in the osmotic pressure within star polymers near the overlap concentration causes a soft repulsion between stars. Looking at the series of molecules containing 24 arms of d_5-PMMA, we see the effect of core architecture. In our star branched copolymer, G1-24, this osmotic repulsion is indicated by a peak in the scattering profile. In the case of copolymer G3-24, the branching junctures creating the G3 core allow the polymer chains to be more uniformly distributed within the core, hence relaxing the osmotic repulsion and leading to a weaker repulsion and only an inflection in the scattering profiles. The intermediate G2 core architecture of copolymer G2-24 still has sufficient osmotic repulsion to develop a peak in the scattering profile. To further elucidate the effect of core architecture on the interactions between the copolymers, we will decouple the shape and interactions of the different PCL cores in section III.3. The upturn in the scattering at low q is not fully understood, although it does indicate the presence of larger structures, most likely some aggregates or imperfect single molecules. This phenomenon has been seen for dendritic structures and has been attributed to weak attractive interactions between molecules with imperfect structures.[51] They reported that, by eliminating the lowest q values showing the upturn, the analysis could be successfully performed on the remaining data. We have used this same approach with our data and have not used these first few points in our analysis when the upturn was present.

To better illustrate the different scattering regimes, we show the scattering profile normalized by volume fraction for copolymer G1-12 in Figure 3. From Figure

Table 2. PCL Core Parameters from Dilute Solution Data Analyses

			R_g (nm)		root g-factors	
copolymer	ν	P	Guinier	Beaucage[a]	$(g_s)^{1/2}$	$(g_3)^{1/2}$
G1-12	0.52	1.92	7.5	8.9	0.49	
G2-12	0.69	1.45	8.0	8.5	0.67	0.74
G1-24	0.60	1.67	6.6	7.8	0.35	
G2-24	0.67	1.49	8.0	8.7	0.49	0.65
G3-24	0.65	1.54	12.7	9.8	0.67	0.60

[a] Fit performed without the polymeric constraint.

3 we see that the normalized scattering profiles depend on constants and V_W (which should be fixed for a given copolymer), the form factor, and the structure factor ($d\Sigma/d\Omega(q)/\phi = ((\Delta\rho)^2/N_A)V_W(P(q)S(q))$). In dilute solutions, the interactions between the polymers will be negligible, leading to a structure factor of unity over the entire q range and therefore a profile dominated by the form factor as shown for the dilute solution of copolymer G1-12. In this profile, the low-q regime, or Guinier regime, gives information about the overall size of the cores. As the concentration is increased, the structure factor will show its effect on the profile in the q range over which interactions are relevant. These effects are seen in the low-q regime and in the crossover regime. It should be noted that the intermediate-q scattering, reflecting contributions from scattering due to monomer correlations (essentially a semidilute polymer solution), is independent of the polymer concentration and exhibits the characteristic power law decay related to the fractal dimension (P) and Flory scaling exponent ($\nu \sim P^{-1}$) of the polymers within the core.

III.2. Dilute Solution Analysis. We can learn more about the effects of architecture by quantitative analysis of the key features of the scattering profiles. We consider the dilute solution data in the intermediate- and low-q regimes. By looking at the intermediate-q ($\pi R_g^{-1} < q < l_p^{-1}$, where l_p is the persistence length of polymer) dilute solution scattering data, we assess the conformation of the polymer chains that comprise the copolymer cores. This scattering regime contains information that can yield the Flory exponent and fractal dimension of the system, which are two important parameters to consider when studying hyperbranched architectures.[52,53] The power law behavior is indicated by the linear region at intermediate-q scattering in a double-logarithmic representation of the data as shown for G1-12 in Figure 3. A least-squares fit to this power law behavior provides the fractal dimensions P or $1/\nu$, given in Table 2.

The values we obtained for ν between 0.52 and 0.69 are near the Θ and good solvent limits (0.50 and 0.60, respectively), with those exceeding the good solvent value indicating chain stretching. The G1-12 star polymer architecture shows a ν value of 0.52, indicating the crowding of the chains at the central core results in a Flory exponent typical of a semidilute polymer solution. Thus, the connectivity in the core of this architecture leads to ideal chain configurations. When the star arm functionality increases to 24 as for G1-24, the core chains become stretched from their ideal conformation due to the high connectivity of chains to the central branching juncture, resulting in a higher Flory exponent of 0.60 as predicted by scaling analysis.[9] The architectures of G2-12, G2-24, and G3-24 contain branching junctures outside of the central juncture at the core and all show similar ν values of 0.69, 0.67, and 0.65, respectively. These values are higher than the anticipated value for polymer chains swollen in a good solvent, indicating that the branching junctures play an important role in the Flory exponent of these architectures.

Investigations of hyperbranched structures have shown that the Flory exponent is related to branching architecture. In dendrimeric structures with high branching density, the Flory exponent was found to be 0.33, indicating a compact space-filling structure with a fractal dimension of 3.[52] A hyperbranched system prepared in a one-step polymerization of AB_2 monomeric units showed a fractal dimension of 2.2 (ν of 0.45).[53] Finally, for a randomly branched system a fractal dimension of 2.28 (ν of 0.44) is anticipated.[54] While our structures have successive branching junctures emanating from a core in a well-defined dendrimer-like fashion, they also have polymeric chains connecting these branching junctures unlike typical dendrimers. In this way, the cores of our systems are analogous to polymer networks or swollen gels rather than typical dendrimers or randomly branched structures.

The conformation of polymer chains in a network or swollen gel is a classical problem in polymer physics[2,55] that has still not been fully resolved. Recent modeling[56−58] has challenged the classical picture of the swelling in polymer gels given by the Flory−Rehner theory[2] and deGennes' c^* theorem.[55] While each of these studies predicts slightly different values of the Flory exponent, they all predict ν greater than or equal to the swollen polymer chain value of 0.60. Our values of 0.65−0.69 lie in the range of ν values predicted by the theories of 0.60−0.72, indicating that the PCL cores show properties similar to those predicted for network and swollen gel structures. While we anticipate that most of the polymer chains between junctures behave as typical swollen chains, the junctures create topological constraints and thus prohibit this behavior from persisting throughout the entire structure. Thus, confining the junctures to the center of the core (G1) creates a more star branched structure, while distributing the junctures throughout the core more closely resembles a swollen gel.

To assess the overall dimensions of the PCL cores of the dendrimer-like star copolymer series, we apply the Guinier approximation to the low-q regime of the dilute solution data. In this approximation in the limit of small qR_g, the data should follow the expression given for the form factor of a sphere based on a series expansion:[59]

$$I(q) \approx \phi V_W \exp\left(-\frac{q^2 R_g^{\ 2}}{3}\right) \tag{3}$$

Hence, a plot of $\ln[I(q)]$ vs q^2 is linear at small q with a slope directly related to the radius of gyration, R_g, of the cores of the copolymer molecules. We perform linear least-squares fits to (3) to obtain the PCL core R_g values as presented in Table 2. The Guinier fits show good linearity, indicating the chosen scattering regime is well approximated by (3). However, the results obtained from this analysis must be carefully considered, as they are sensitive to the number of data points included in the fit and assume that the scattering data can be represented by a spherical form factor. To ensure we have accurate measures of the core sizes, we will additionally apply a model form factor to validate our R_g measurements.

To verify our Guinier results and to allow us to decompose the total scattering intensity into the form factor, $P(q)$, and structure factor, $S(q)$, we fit model form factor functions to our dilute solution data that will in turn be used to calculate the structure factor in section III.3. Fitting SANS data with model form factor expressions has shown to be a valuable analysis technique and has been the subject of recent reviews.[60−62] While many form factor expressions have been derived for common shapes, such as spheres and rods,[63] starlike polymers present a complex shape with multiple length scales. One characteristic length scale in these systems is the overall dimension of the individual molecules given by R_g. As theoretically described by Daoud and Cotton,[9] there are also length scales that describe the inhomogeneous blob structure within the star arms. Since the architecture of these molecules produces repulsive interactions, there is yet another imposed length scale in the system that describes the range of these interactions.

By employing a model form factor, we can fit our dilute solution data over the entire q range rather than being limited to only the low-q data applicable to the Guinier analysis. We apply an analytical form factor developed for scattering from polymeric mass fractals developed by Beaucage.[64−66] This model combines the low-q Guinier regime described by (3) with an intermediate-q power law regime where scattering is from a semidilute polymer solution. As our data show the Guinier regime at low q and the power law regime at intermediate q, the difficulty in modeling our data arises in the reproduction of the crossover regime between these two limits. In this crossover regime the subtleties of the polymer architecture become apparent, and therefore, it is important to obtain an accurate model for this regime. Beyond the intermediate-q regime showing the power law scaling of the polymeric chains, the data show the expected high-q power law scaling of q^{-1}, indicating the local rigidity of the polymer backbones. As we are not interested in this regime, we truncate the data before q reaches the inverse of the persistence length, with $l_p \sim 1$ nm for typical carbon backbone polymer chains.

In modeling of star polymer scattering data, a form factor given by Dozier and co-workers has been employed extensively.[17] This model has been used in star polymer studies to examine both the dilute solution properties and the scaling relationships involving the star arm length and functionality (i.e., number of star arms).[16−18,67] In this form factor, they propose that the Guinier scattering of spherical stars in the low-q regime and the Fourier transform of the mass−mass correlation function in the intermediate-q regime can be summed to obtain the form factor.

$$V_W P(q) = V_W \exp\left(-\frac{q^2 R_g^{\ 2}}{3}\right) + \frac{\alpha}{q\xi}\,\frac{\sin\,[\mu\,\tan^{-1}(q\xi)]}{(1+(q\xi)^2)^{\mu/2}} \quad (4)$$

In this expression, μ is equal to $1/\nu - 1$, ξ is an average blob size, and α is a fitting parameter. Typically, ν is fixed and V_W, R_g, α, and ξ are left as adjustable parameters. In this functional form, the second term describing the intermediate-q regime does not vanish as q goes to zero, resulting in underestimation of V_W.[14] Thus, the relative magnitudes of the two terms in (4) must be analyzed when considering the V_W parameters obtained by fitting data to this expression. Furthermore, the interpretation of the parameters α and ξ is difficult. When we applied fits of our data to (4), we found satisfactory recreation of the features of the scattering profile; however, the known problems regarding the form of the intermediate-q region and the difficulties in interpreting the parameters obtained using this model prevent us from presenting these results.

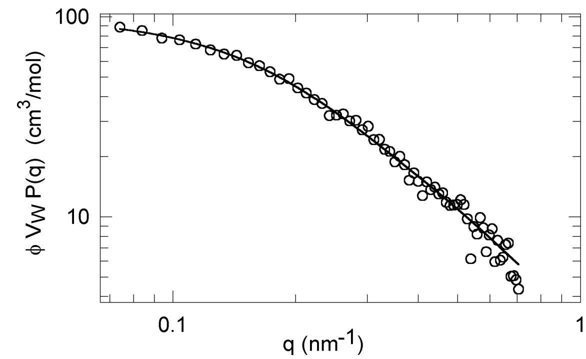

Figure 4. Form factor for copolymer G1-12 at 0.2 wt % (open circles) is shown along with the model fits obtained from the Beaucage expression (solid line).

The Beaucage form factor uses the same functional form to describe the low-q scattering as in the Dozier expression, but a different expression employing the error function and gamma function is used for the intermediate-q scattering.

$$V_W P(q) = G\,\exp\left(-\frac{q^2 R_g^{\ 2}}{3}\right) + B\left(\frac{1}{q^*}\right)^P \quad (5)$$

In this expression q^* is equal to $q/[\mathrm{erf}(kqR_g/6^{1/2})]^3$. In the definition of q^*, the empirical constant k takes into account the approximations used to describe the low-q power law limit and is set to the value for polymeric mass fractals of 1.06.[66] The values of B and G weigh the magnitudes of the two terms in (5) and can be related to one another using the polymeric constraint assumption where $B = (GP/R_g^{\ P})\Gamma(P/2)$. We perform fits to this model function with P fixed to the values obtained in our analysis of the intermediate-q regime and with the adjustable parameters G and R_g. When we fit the data using the polymeric constraint assumption to relate G and B, we find poor results for some of the copolymers in the crossover regime as indicated by nonrandom trends in the residuals. In particular, the polymer architectures with 24 arms (G1-24, G2-24, and G3-24) showed poor results, perhaps due to the fact that the short chains between branching junctures within the PCL cores may not be long enough to behave as polymeric segments. By relaxing the polymeric constraint condition and including B as an additional fitting parameter, we obtain good fits for all the copolymers as indicated by the low magnitude and randomness of the residuals. Thus, we present only the parameters obtained from the Beaucage model without the polymeric constraint. A representative fit of the Beaucage model is shown in Figure 4 along with the data for copolymer G1-12.

We consider the information gained from the Guinier and Beaucage model form factor analyses. We compare the values for the PCL core R_g calculated by these techniques. The Guinier and Beaucage results are consistent with one another, with the exception of G3-24. In this case, the Guinier results predicted a much larger R_g than the Beaucage fit. Generally, the Beaucage results show larger radii and a smaller variation in the R_g values of the PCL cores through the copolymer series versus the Guinier results. This could be due to the effects of the second term in (5) even in the low-q regime. Although we find that the first several points are dominated by the Guinier term in the Beaucage fits, the crossover to the power law regime is quite sharp and may extend into points of the Guinier regime. Thus, the two models truncate the Guinier regime at different points, causing the slight discrepancies in the results obtained.

We consider the effects of the core branching architecture PCL core radii. We anticipate that increasing the number of branching junctures in a system will result in more compact structures. In our copolymer series for a given arm architecture, the number of branching junctures in each copolymer is identical, as shown in Figure 1. Thus, it is the placement of the junctures within the structures that impacts the size of these cores. Generally, we find that the effects are more apparent for more constrained structures. We expect that the 24-arm copolymers will be more compact than their 12-arm analogues. This is the case for the G1 star cores while the G2 cores show nearly the same size. A comparison of the two 12-arm copolymers (G1-12 and G2-12) shows they essentially have the same core R_g, indicating branch juncture placement within structures of low branching density does not strongly impact the resulting R_g. The effect of branch juncture distribution is clearly seen in the 24-arm copolymers. For these copolymers, we see that having branches confined to the central core results in more compact structures. Thus, the architecture of G1-24 with 24 PCL chains centrally connected results in the most compact architecture of the series as indicated by the smallest PCL core R_g of the series. Conversely, moving the branching away from the center of the core causes it to expand. With the most distributed branching junctures in the series, only six chains emanate from the central core of G3-24 and then branch twice to create 24 arms, resulting in the largest PCL core R_g of the series.

We can interpret these results further by considering the classical Zimm and Stockmayer analysis defining the g-factor (or contraction factor) of branched structures.[1]

$$g = \left. \frac{{R_{g,b}}^2}{{R_{g,lin}}^2} \right|_M \tag{6}$$

Here, the g-factor relates the radii of gyration of a polymer of molecular weight M in a branched (b) architecture versus its isomeric linear analogue (lin). Generally speaking, by introducing branching into a system, the R_g of the polymer will be reduced. The nature of the branching will determine the magnitude of this reduction, and analytical expressions have been developed to predict the g-factor for different branching architectures. One key parameter in determining the g-factor is the functionality of the branching in a system (i.e., the number of chains connected at each juncture). Other parameters impacting the g-factor include the branch density (i.e., the number of branch junctures in the system) and the length of the polymeric chains between branches. Star polymer architectures exhibit one limit of branching functionality, with all of the branching functionalized at a single juncture. For regular star polymers with f arms, the branching functionality is f and the g-factor, g_s, can be predicted.[40]

Table 3. *g*-factor Analysis for PCL Cores

copolymer	f_c	m	t	g_s	g_3
G1-12	12	50	12	0.24	
G2-12	6	33	18	0.44	0.55
G1-24	24	25	24	0.12	
G2-24	12	17	36	0.24	0.43
G3-24	6	14	42	0.44	0.36

$$g_s = \frac{3f - 2}{f^2} \tag{7}$$

In the opposite limit, trifunctional branching (like that in many dendrimers) creates a very different branching geometry. In the analytical prediction of the g-factor for a randomly branched system with trifunctional branching, the only parameter is the number of branches, denoted as n. Hence, a branched polymer comprised of n branches each of m monomer units in length will have an overall degree of polymerization x given by $x = m \times n$ and a g-factor, g_3:[40]

$$g_3 = \left[\left(1 + \frac{n}{7}\right)^{1/2} + \frac{4n}{9\pi}\right]^{-1/2} \tag{8}$$

Our G2 and G3 PCL cores are intermediate between star and trifunctionally branched architectures and thus should have g-factors that reflect the presence of these two different branching architectures. The g-factors predicted by (7) and (8) can be considered as limits for these hybrid systems. We denote the total number of branching units emanating from the center of the core f_c, and thus, the PCL cores have an f_c functional starlike central core. Each of the f_c branches emanating from this core then exhibits trifunctional branching at one or two successive junctures to create the G2 or G3 structure. The number of trifunctional branches in the system (i.e., branches not connected directly to the central core), denoted n_3, can be calculated as the total number of branches, t, minus those exhibiting starlike branching, f_c. Thus, we can evaluate (7) and (8) with the parameters f_c and n_3, respectively, to obtain the g-factors shown in Table 3.

Because of the low-q limits of SANS, it is not feasible to measure the R_g of a PCL linear chain of the same molecular weight as the PCL cores to obtain absolute g-factors. From (6) we can see that R_g for a branched structure should be equal to the square root of the g-factor. Thus, we can compare the root g-factors to the R_g data as shown in Table 2 to consider the ability of (7) and (8) to predict the contraction in the hybrid branched PCL cores. The root g-factor values obtained for the star architectures predict G1-24 to be the most compact structure and G1-12 to be the second smallest as consistent with the Guinier results. Because of the hybrid nature of the G2 and G3 cores, the actual root g-factor should be between the values predicted for star and trifunctional branching. The root g-factor values predict G2-12 to be larger than we observe. However, the root g-factors accurately predict the large radii of G3-24. In fact, the root g-factor values of the 24-arm copolymers are in excellent quantitative agreement with the trends in the Beaucage radii. To explore quantitative relationships for hybrid architectures in detail, a broader range of architectures would be desired. However, we find g-factors to be valuable tools in qualitatively predicting the effects of branching in copolymer systems using analytically predicted values for relevant branching geometries.

III.3. Experimental Structure Factors. Using the results from the model form factor fits, we can obtain experimental structure factors by dividing out the form factor, volume fractions, and other necessary constants.

$$S(q) = \left(\frac{1}{V_W P(q)}\right)\left(\frac{I(q)}{\phi}\right) = \left(\frac{N_A}{V_W P(q)(\Delta\rho)^2}\right)\left(\frac{1}{\phi}\frac{d\Sigma^{coh}}{d\Omega}(q)\right) \tag{9}$$

To apply this analysis, we must make the decoupling approximation and assume centrosymmetry as discussed above.[49] Additionally, we assume that the form factor for these cores does not change with increasing concentration.[17] Although we do anticipate changes to the form factor as the overlap concentration is exceeded, we assume that the PCL cores will not change shape much within these concentration regimes and that the first bracketed term in (9) remains constant for the concentration regime that we are studying.[17] This approach has been successfully applied for many star polymer systems to obtain experimental structure factors.[14−16,18] The approximation of the dilute solution form factor is fairly robust when the copolymer solutions are below the overlap concentration, which is the certainly the case for the 0.5 and 1 wt % solutions. Once the overlap concentration is exceeded, we would expect deviations from the dilute solution form factor to arise due to shrinkage of the cores; slight isotropic osmotic compression would not change the overall shape of the structure factor profile significantly.[18] Studies of 12-arm stars with relatively low molecular weight arms comparable to our structures have shown no deviation in the form factor even well above the overlap concentration.[68] We are cautious in our quantitative analysis of the structure factor intensity data due to concerns regarding the use of the dilute solution form factor to obtain the structure factor.

The structure factor data required some treatment to quantitatively recover the correct asymptote of unity at high q. The scattering due to the solvent was subtracted on a volume fraction basis; however, incoherent scattering due to the copolymer must also be eliminated from the scattering profiles. The incoherent scattering from each copolymer sample is difficult to predict as there are contributions due to both the disorder of the nuclei and the uncorrelated spins of the neutrons and the nuclei of the copolymer.[63] We determine the incoherent scattering corrections by ensuring the structure factor reaches a plateau at high q. We find the incoherent scattering only attributes to a small fraction of the total scattering intensity. A second multiplicative correction factor is used to ensure that the structure factor reaches the correct asymptote at high q. As the solutions we are studying are in some cases quite dilute, this factor allows for us to account for deviations in the actual solution concentration from those measured during sample preparation. As these correction factors are close to unity (0.3−1.4), this treatment is not a concern for our qualitative analysis of the structure factor intensities. The experimental structure factors are shown for copolymers G1-12, G1-24, G2-12, and G2-24 in Figure 5.

The presence of a structure factor peak near the overlap concentration occurs for star polymers of a critical functionality, although this critical functionality cannot be accurately predicted.[50] The absence of higher order structure factor peaks indicates that only short-range liquidlike structure exists. In our systems, the experimental structure factors show evidence of liquid-like structuring. The structure factor peak is absent or weak at the lowest concentrations studied. As the concentration is increased, the peak develops and becomes more pronounced to a point beyond which further increase in concentration causes the peak to decay. While not all of the copolymers show a prominent peak in their structure factor with concentration, they all exhibit a correlation hole in their structure factors at low q with increasing concentration. The presence of a correlation hole at low q unaccompanied by a structure factor peak is consistent with other studies of star and dendrimer polymers.[17,69] This phenomenon is attributed to the soft-core nature of the repulsions between molecules,[17] indicating that the effective pair potential between the molecules depends only weakly on their separation.[13] Hence, the polymer chains comprising these molecules may interpenetrate or contract in response to crowding by neighboring molecules as they are "soft".

In our system we have two architectural variables contributing to the interactions of the molecules that lead to structure. The star arm length dictates the length scales over which the interactions are present between molecules, and the core architecture (i.e., functionality and branching) determines the osmotic pressure within the individual molecules which in turn leads to structuring. The magnitude of the structure factor peak indicates the degree of structure occurring in a system. Because of our data correction treatment, we must be cautious in any quantitatively analysis the peak heights. For star polymers it is predicted that the peak height in the structure factor will scale with the arm functionality raised to the $^3/_2$ power.[16] While we only have two arm functionalities and cannot test this scaling, we do see that greater functionality leads to greater peak heights as found in other low-functionality star systems.[16] The onset of crystalline order is seen when the magnitude of the structure factor peak exceeds a value of 2.85.[70] The structure factor peaks in our systems do not approach the crystalline limit nor do we see higher order peaks, indicating that the system remains in the liquid state. We do see that that the constraint of the star core of copolymers G1-12 and G1-24 leads to enhanced structuring as compared to the G2 and G3 cores. While there is still some evidence of liquidlike structuring of the G2 cores, the G3 core exhibited no structure factor peak at all, again reinforcing that core constraint causes the structuring phenomena in these systems.

The positions of the peaks in the structure factor reveal the characteristic spacing between the scattering centers. We can estimate this spacing, d, from the position of the structure factor peak, q_{max}, using the simple relation $d \sim 2\pi/q_{max}$, assuming no specific arrangement of the molecules. We can then see how the molecules pack as we increase the volume fraction of copolymer in the solution. In Figure 6 we compare this spacing to that arising from a uniform distribution of scattering centers in space, $d_{uni} = (N_p)^{-1/3}$ where N_p is the copolymer number density.[71]

First we consider the results for the low-concentration structure factor data. At these dilute concentrations, the copolymers are not in contact with one another, and

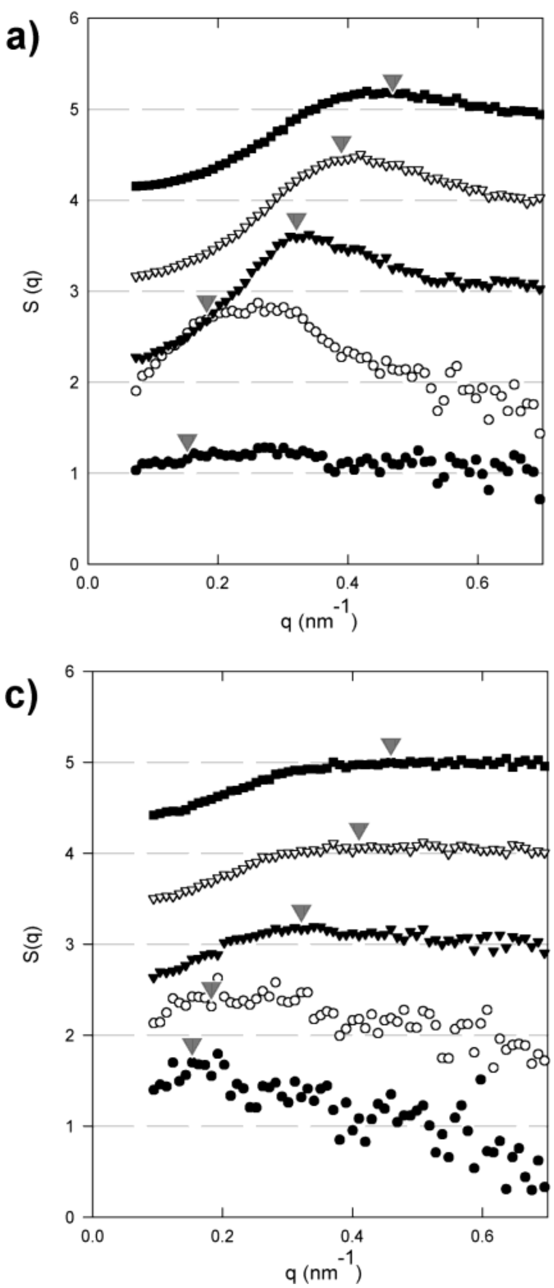

Figure 5. Experimental structure factors are shown for (a) G1-12, (b) G1-24, (c) G2-12, and (d) G2-24. The copolymer concentrations in each plot are approximately 0.5 wt % (closed circles), 1 wt % (open circles), 5 wt % (closed triangles), 10 wt % (open triangles), and 15 wt % (closed squares) and are shown with the highest concentration at the top of each plot. The plots in each graph are offset by the following constants: 0.5 wt % (0), 1 wt % (1), 5 wt % (2), 10 wt % (3), and 15 wt % (4). The gray triangle indicates the *q* value corresponding to the characteristic spacing for a uniform distribution for each data set.

hence the structure factor data show only minor, broad peaks. These peaks indicate that there are weak interactions between the copolymers and poor localization of the copolymers. The shape of these peaks precludes accurate determination the peak positions; however, the *q* value that would correspond to the characteristic spacing for a uniform distribution of molecules is located just after the steep rise out of the correlation hole at low *q* in these structure factors in copolymers G1-12, G1-24, G2-12, and G2-24, as indicated in Figure 5.

Since the concentrations of the copolymer solutions are near the overlap concentration, they all yield structure factor peak locations obeying the uniform distribution characteristic spacing. This behavior for the peak positions of the structure factor continues regardless of copolymer architecture through the entire concentration regime studied; however, in the high-concentration regime the presence of a peak in the structure factor remains only for the copolymers with the most constrained cores, G1-12 and G1-24. Hence, the copolymer architecture controls the degree of liquidlike structure and the concentration regimes over which this structuring will occur while the nature of the packing of the copolymers is independent of copolymer architecture.

IV. Conclusions

Dilute solution analyses of these dendrimer-like star copolymers in shell match solvent show that the branching within the core of the molecule impacts its overall size and the Flory exponent of the chains comprising the core. We find that the branching architecture creates

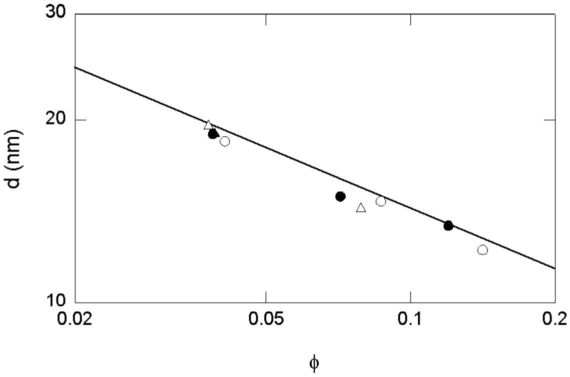

Figure 6. Characteristic spacing, *d*, is shown for copolymers G1-12 (closed circles), G1-24 (open circles), G2-12 (closed triangles), and G2-24 (open triangles) as a function of volume fraction copolymer, ϕ. The line indicates the behavior for uniformly distributed molecules.

starlike chain conformations in the G1 cores while chain behavior analogous to that in networks and swollen gels is found for the G2 and G3 cores. A *g*-factor analysis indicates the nature of the branching can be used to qualitatively predict the contraction of a branched architecture versus its linear isomer. At higher concentrations, the copolymer cores exhibit liquidlike structure when the core density distribution is inhomogeneous. This structure appears to be enhanced with increasing star arm functionality; however, a distribution of the branching junctures within the core allows for a more homogeneous density distribution of the polymer segments over a larger core, relieving the osmotic repulsion and weakening the structuring tendency. Although the effect of star functionality on solution structuring has been explored,[16,18] the effect of core architecture on the structure of otherwise identical star molecules has not been explicitly investigated. Our findings are consistent with an ordering phenomenon driven by inhomogeneous distribution of polymer segments created by the distribution of branching points in these copolymer architectures. In other more complex hyperbranched architectures, we expect that additional factors such as steric packing constraints and specific interactions (e.g., electrostatic repulsions, H-bonding) may also contribute to their solution structure. The presence of both architecture dependent and independent properties within a series of molecules creates an interesting system with great versatility for technological applications. These molecules can have very similar properties in some regards while simultaneously possessing other features dependent on architecture that could be invoked as necessary for a particular application. By creating a deeper fundamental understanding of the relationships between the architecture of hyperbranched systems and their properties, we come one step closer to exploiting these molecules for advanced technologies.

Acknowledgment. We acknowledge support for this work from the NSF Center for Polymer Interfaces and Macromolecular Assemblies (CPIMA), Grant DMR-9808677. We acknowledge the support of the National Institute of Standards and Technology, U.S. Department of Commerce, in providing facilities used in this work. This material is based upon activities supported by the National Science Foundation under Agreement DMR-9986442. We acknowledge the support of Institut Laue-Langevin for providing facilities used in this work.

References and Notes

(1) Zimm, B. H.; Stockmayer, W. H. *J. Chem. Phys.* **1949**, *17*, 1301−1314.
(2) Flory, P. J. *Principles of Polymer Chemistry*; Cornell University Press: Ithaca, NY, 1953.
(3) Tomalia, D. A.; Baker, H.; Dewald, J.; Hall, M.; Kallos, G.; Martin, S.; Roeck, J.; Ryder, J.; Smith, P. *Polym. J.* **1985**, *17*, 117−132.
(4) Hawker, C. J.; Fréchet, J. M. J. *Macromolecules* **1990**, *23*, 4726−4729.
(5) Hawker, C. J.; Fréchet, J. M. J. *J. Am. Chem. Soc.* **1990**, *112*, 7638−7647.
(6) Fréchet, J. M. J. *Proc. Natl. Acad. Sci. U.S.A.* **2002**, *99*, 4782−4787.
(7) Matthews, O. A.; Shipway, A. N.; Stoddart, J. F. *Prog. Polym. Sci.* **1998**, *23*, 1−56.
(8) Roovers, J.; Comanita, B. *Adv. Polym. Sci.* **1999**, *142*, 179−228.
(9) Daoud, M.; Cotton, J. P. *J. Phys. (Paris)* **1982**, *43*, 531−538.
(10) Birshtein, T. M.; Zhulina, E. B. *Polymer* **1984**, *25*, 1453−1461.
(11) Birshtein, T. M.; Zhulina, E. B.; Borisov, O. V. *Polymer* **1986**, *27*, 1078−1086.
(12) Adam, M.; Fetters, L. J.; Graessley, W. W.; Witten, T. A. *Macromolecules* **1991**, *24*, 2434−2440.
(13) Likos, C. N.; Löwen, H.; Watzlawek, M.; Abbas, B.; Jucknischke, O.; Allgaier, J.; Richter, D. *Phys. Rev. Lett.* **1998**, *80*, 4450−4453.
(14) Likos, C. N.; Löwen, H.; Poppe, A.; Willner, L.; Roovers, J.; Cubitt, B.; Richter, D. *Phys. Rev. E* **1998**, *58*, 6299−6307.
(15) Marques, C. M.; Izzo, D.; Charitat, T.; Mendes, E. *Eur. Phys. J. B* **1998**, *3*, 353−358.
(16) Willner, L.; Jucknischke, O.; Richter, D.; Farago, B.; Fetters, L. J.; Huang, J. S. *Europhys. Lett.* **1992**, *19*, 297−303.
(17) Dozier, W. D.; Huang, J. S.; Fetters, L. J. *Macromolecules* **1991**, *24*, 2810−2814.
(18) Richter, D.; Jucknischke, O.; Willner, L.; Fetters, L. J.; Lin, M.; Huang, J. S.; Roovers, J.; Toporovski, C.; Zhou, L. L. *J. Phys. IV* **1993**, *3*, 3−12.
(19) Groh, B.; Schmidt, M. *J. Chem. Phys.* **2001**, *114*, 5450−5456.
(20) Likos, C. N.; Schmidt, M.; Löwen, H.; Ballauff, M.; Pötschke, D.; Lindner, P. *Macromolecules* **2001**, *34*, 2914−2920.
(21) Seghrouchni, R.; Petekidis, G.; Vlassopoulos, D.; Fytas, G.; Semenov, A. N.; Roovers, J.; Fleischer, G. *Europhys. Lett.* **1998**, *42*, 271−276.
(22) Uhrich, K. *Trends Polym. Sci.* **1997**, *5*, 388−393.
(23) Supattapone, S.; Nguyen, H. O. B.; Cohen, F. E.; Prusiner, S. B.; Scott, M. R. *Proc. Natl. Acad. Sci. U.S.A.* **1999**, *96*, 14529−14534.
(24) De Jesús, O. L. P.; Ihre, H. R.; Gagne, L.; Fréchet, J. M. J.; Szoka, F. C. *Bioconjugate Chem.* **2002**, *13*, 453−461.
(25) Ihre, H. R.; De Jesús, O. L. P.; Szoka, F. C.; Fréchet, J. M. J. *Bioconjugate Chem.* **2002**, *13*, 443−452.
(26) Hecht, S.; Vladimirov, N.; Fréchet, J. M. J. *J. Am. Chem. Soc.* **2001**, *123*, 18−25.
(27) Hecht, S.; Ihre, H.; Fréchet, J. M. J. *J. Am. Chem. Soc.* **1999**, *121*, 9239−9240.
(28) Freeman, A. W.; Koene, S. C.; Malenfant, P. R. L.; Thompson, M. E.; Fréchet, J. M. J. *J. Am. Chem. Soc.* **2000**, *122*, 12385−12386.
(29) Harth, E. M.; Hecht, S.; Helms, B.; Malmstrom, E. E.; Fréchet, J. M. J.; Hawker, C. J. *J. Am. Chem. Soc.* **2002**, *124*, 3926−3938.
(30) Hedrick, J. L.; Magbitang, T.; Connor, E. F.; Glauser, T.; Volksen, W.; Hawker, C. J.; Lee, V. Y.; Miller, R. D. *Chem. Eur. J.* **2002**, *8*, 3308−3319.
(31) Hedrick, J. L.; Miller, R. D.; Hawker, C. J.; Carter, K. R.; Volksen, W.; Yoon, D. Y.; Trollsås, M. *Adv. Mater.* **1998**, *10*, 1049−1053.
(32) Heise, A.; Nguyen, C.; Malek, R.; Hedrick, J. L.; Frank, C. W.; Miller, R. D. *Macromolecules* **2000**, *33*, 2346−2354.
(33) Ballauff, M. In *Dendrimers III: Design, Dimension, Function*; Vögtle, F., Ed.; Top. Curr. Chem. 212; Springer Publishing: New York, 2001; pp 177−194.
(34) Topp, A.; Bauer, B. J.; Prosa, T. J.; Scherrenberg, R.; Amis, E. J. *Macromolecules* **1999**, *32*, 8923−8931.
(35) Topp, A.; Bauer, B. J.; Klimash, J. W.; Spindler, R.; Tomalia, D. A.; Amis, E. J. *Macromolecules* **1999**, *32*, 7226−7231.
(36) Prosa, T. J.; Bauer, B. J.; Amis, E. J.; Tomalia, D. A.; Scherrenberg, R. *J. Polym. Sci., Part B: Polym. Phys.* **1997**, *35*, 2913−2924.
(37) Prosa, T. J.; Bauer, B. J.; Amis, E. J. *Macromolecules* **2001**, *34*, 4897−4906.

(38) Hawker, C. J.; Malmström, E. E.; Frank, C. W.; Kampf, J. P. *J. Am. Chem. Soc.* **1997**, *119*, 9903−9904.
(39) Trollsås, M.; Atthof, B.; Würsch, A.; Hedrick, J. L.; Pople, J. A.; Gast, A. P. *Macromolecules* **2000**, *33*, 6423−6438.
(40) Burchard, W. *Adv. Polym. Sci.* **1999**, *143*, 113−194.
(41) Hedrick, J. L.; Trollsås, M.; Hawker, C. J.; Atthoff, B.; Claesson, H.; Heise, A.; Miller, R. D.; Mecerreyes, D.; Jérôme, R.; Dubois, P. *Macromolecules* **1998**, *31*, 8691−8705.
(42) Trollsås, M.; Claesson, H.; Atthoff, B.; Hedrick, J. L. *Angew. Chem., Int. Ed.* **1998**, *37*, 3132−3136.
(43) Trollsås, M.; Hedrick, J. L. *J. Am. Chem. Soc.* **1998**, *120*, 4644−4651.
(44) Trollsås, M.; Hedrick, J. L.; Mecerreyes, D.; Dubois, P.; Jérôme, R.; Ihre, H.; Hult, A. *Macromolecules* **1998**, *31*, 2756−2763.
(45) Trollsås, M.; Kelly, M. A.; Claesson, H.; Siemens, R.; Hedrick, J. L. *Macromolecules* **1999**, *32*, 4917−4924.
(46) Stancik, C. M.; Pople, J. A.; Hedrick, J. L.; Kline, S. R.; Gast, A. P. NIST Experimental Report, 2000.
(47) *SANS Data Reduction and Imaging Software*; Cold Neutron Research Facility, NIST: Gaithersburg, MD, 1996.
(48) Ghosh, R. E.; Egelhaaf, S. U.; Rennie, A. R. *A Computing Guide for Small-Angle Scattering Experiments*; Institut Max von Laue Paul Langevin: Grenoble, France, 2000.
(49) Pedersen, J. S. *J. Chem. Phys.* **2001**, *114*, 2839−2846.
(50) Witten, T. A.; Pincus, P. A.; Cates, M. E. *Europhys. Lett.* **1986**, *2*, 137−140.
(51) Pötschke, D.; Ballauff, M.; Lindner, P.; Fischer, M.; Vögtle, F. *Macromolecules* **1999**, *32*, 4079−4087.
(52) Scherrenberg, R.; Coussens, B.; van Vliet, P.; Edouard, G.; Brackman, J.; de Brabander, E.; Mortensen, K. *Macromolecules* **1998**, *31*, 456−461.
(53) Geladé, E. T. F.; Goderis, B.; de Koster, C. G.; Meijerink, N.; van Benthem, R.; Fokkens, R.; Nibbering, N. M. M.; Mortensen, K. *Macromolecules* **2001**, *34*, 3552−3558.
(54) King, S. M. In *Modern Techniques for Polymer Characterisation*; Pethrick, R. A., Dawkins, J. V., Eds.; John Wiley & Sons Ltd.: New York, 1999; pp 171−232.
(55) de Gennes, P. G. *Scaling Concepts in Polymer Physics*; Cornell University Press: Ithaca, NY, 1979.
(56) Pütz, M.; Kremer, K.; Everaers, R. *Phys. Rev. Lett.* **2000**, *84*, 298−301.
(57) Sommer, J. U.; Russ, T.; Brenn, R.; Geoghegan, M. *Europhys. Lett.* **2002**, *57*, 32−38.
(58) Sukumaran, S. K.; Beaucage, G. *Europhys. Lett.* **2002**, *59*, 714−720.
(59) Glatter, O.; Kratky, O. *Small-Angle X-ray Scattering*; Academic Press: London, 1982.
(60) Castelletto, V.; Hamley, I. W. *Curr. Opin. Colloid Interface Sci.* **2002**, *7*, 167−172.
(61) Pedersen, J. S. *Adv. Colloid Interface Sci.* **1997**, *70*, 171−210.
(62) Pedersen, J. S.; Svaneborg, C. *Curr. Opin. Colloid Interface Sci.* **2002**, *7*, 158−166.
(63) Higgins, J. S.; Benoit, H. C. *Polymers and Neutron Scattering*; Clarendon Press: Oxford, 1994.
(64) Beaucage, G.; Schaefer, D. W. *J. Non-Cryst. Solids* **1994**, *172*, 797−805.
(65) Beaucage, G. *J. Appl. Crystallogr.* **1995**, *28*, 717−728.
(66) Beaucage, G. *J. Appl. Crystallogr.* **1996**, *29*, 134−146.
(67) Willner, L.; Jucknischke, O.; Richter, D.; Roovers, J.; Zhou, L. L.; Toporowski, P. M.; Fetters, L. J.; Huang, J. S.; Lin, M. Y.; Hadjichristidis, N. *Macromolecules* **1994**, *27*, 3821−3829.
(68) Huber, K.; Bantle, S.; Burchard, W.; Fetters, L. J. *Macromolecules* **1986**, *19*, 1404−1411.
(69) Ramzi, A.; Scherrenberg, R.; Brackman, J.; Joosten, J.; Mortensen, K. *Macromolecules* **1998**, *31*, 1621−1626.
(70) Hansen, J.; Verlet, L. *Phys. Rev.* **1969**, *184*, 151−161.
(71) Gröhn, F.; Antonietti, M. *Macromolecules* **2000**, *33*, 5938−5949.

MA021450+